Available online at www.sciencedirect.com
SCIENCE DIRECT®
Journal of Nuclear Materials 355 (2006) 136–141
journal of nuclear materials
www.elsevier.com/locate/jnucmat

Characterisation of stainless steel–synroc interactions under hot isostatic pressing (HIPing) conditions

H. Li, Y. Zhang *, P.J. McGlinn, S. Moricca, B.D. Begg, E.R. Vance

Australian Nuclear Science and Technology Organisation, PMB 1, Menai, NSW 2234, Australia

Received 3 January 2006; accepted 2 May 2006

Abstract

Stainless steel/synroc interactions under HIPing conditions (1280 °C/100 MPa/3 h) have been studied. The synroc material was based on the zirconolite-rich ceramic targeted for surplus Pu disposition. A ~300 mm-thick complex reaction interface with 8 distinct layers has been identified. Although the Fe diffusion controlled interactions have changed the microstructures of the synroc phases at the interface, they do not affect the integrity of synroc and are unlikely to have any detrimental effect on this synroc derivative.

1. Introduction

Synroc, a titanate-based ceramic, was first developed in the late 1970s [1,2] for immobilisation of HLW from Purex-type reprocessing of spent nuclear fuels. Since then, various synroc formulations targeting different high-level waste streams have been developed [3,4]. Synroc variations have been developed around synroc-C in which zirconolite ($CaZrTi_2O_7$) and perovskite ($CaTiO_3$) accommodate actinides, Sr and rare earth fission products; hollandite [$Ba(Al,Ti)_2Ti_6O_{16}$] incorporates Cs and Rb, while other fission products such as Tc, Ru, Rh, Pd etc. form very fine metal particles. In the early 1990s, some zirconolite-rich and pyrochlore-rich ($CaATi_2O_7$, A = actinides) formulations were also developed for immobilisation of surplus plutonium [5,6]. Hf and Gd were included in these formulations as neutron absorbers.

Parallel to the synroc formulation development, advanced synroc processing technologies, including hot uniaxial pressing (HUP), sintering, cold crucible induction melting (CCIM) and hot isostatic pressing (HIP), have also been extensively studied [7,8]. HIPing has been widely applied in the last 10 years due to its advantages for processing of high-level radioactive wastes. Firstly, the HIPing process uses sealed stainless steel cans which eliminate radioactive volatile emissions during the high-temperature consolidation process. Subsequently there is no significant amount of secondary waste to deal with and no high temperature off-gas treatment is required other than that arising during lower temperature calcination. Secondly, the HIPing process does not require tight control of the electrical properties, melting temperature, or viscosity of the

* Corresponding author. Tel.: +61 2 9717 9156; fax: +61 2 9543 7179.
E-mail address: yzx@ansto.gov.au (Y. Zhang).

0022-3115/$ - see front matter © 2006 Elsevier B.V. All rights reserved.
doi:10.1016/j.jnucmat.2006.05.014

waste form and therefore can process a wider range of wastes and waste form compositions at higher waste loadings than vitrification.

To achieve good integrity of the waste form and to provide a sealed processing environment, drum-shaped stainless steel cans are used for the waste containment. It is of interest to study the stainless steel/synroc interactions under HIPing conditions and subsequently understand whether such metal/ceramic interactions have any effect on the waste form long-term stability under repository conditions. In the past the main interaction of synroc-C with the stainless steel HIP can was found (unpublished work by some of the authors) to be the build-up of a Cr-rich oxide layer on the can/synroc interface and it was also found that there were no detectable layers of potentially semi-volatile fission products such as Cs or Tc. These ions enter the hollandite and metal alloy phases, respectively [1,2]. However here we report the first detailed characterisation of stainless steel/synroc interactions after HIPing.

2. Experimental

A zirconolite-rich synroc formulation was chosen for this study, with Ce added as the actinide simulant. The detailed oxide composition is given in Table 1. A 10 kg sample was prepared by the oxide route [4], calcined at 700 °C for 2 h, and then HIPed at 1280 °C, 100 MPa for 3 h under an argon atmosphere. The HIP can was made from 2 mm thick 316 stainless steel.

The sample was cut from the HIPed synroc adjoining the stainless steel can. Special care was taken to prevent the delamination of the synroc waste form and the can. The sample was then cross sectionally mounted in epoxy resin, and polished to a 0.25 μm diamond finish.

Table 1
Oxide composition of the zirconolite-rich synroc formulation

Oxide	Wt%
CaO	6.88
BaO	2.34
Gd_2O_3	8.96
Sm_2O_3	0.74
HfO_2	0.86
ZrO_2	21.50
CeO_2	9.77
TiO_2	44.55
Al_2O_3	4.40

Scanning electron microscopy (SEM) was carried out with a JEOL JSM-6300 instrument operated at 15 kV, and fitted with a NORAN Voyager IV X-ray microanalysis system (EDX). Calibrations for microanalysis were carried out using a comprehensive set of standards for quantitative analysis [9].

3. Results and discussion

3.1. Characterisation of the interface region between stainless steel can and synroc

The bulk of the zirconolite-rich synroc sample consisted of four major phases (see Fig. 1), namely zirconolite (70.5%), hollandite (11.5%), rutile (TiO_2, 11%) and a pyrochlore-structured actinide phase (7%). The reaction between the stainless steel can and synroc occurred during HIP processing. Fig. 2 shows the typical microstructure of the reaction interface region (cross section) which can be further divided into eight distinct layers. X-ray elemental mapping was also performed on these regions (Fig. 3).

Layer 1 is the Cr-depleted stainless steel (about 50–60 μm thick). The EDS analysis showed that maximum depletion occurred in the stainless steel near the reaction interface (see Table 2), with the Cr concentration falling from its normal value of ~18 wt% to ~10 wt% adjacent to the reaction

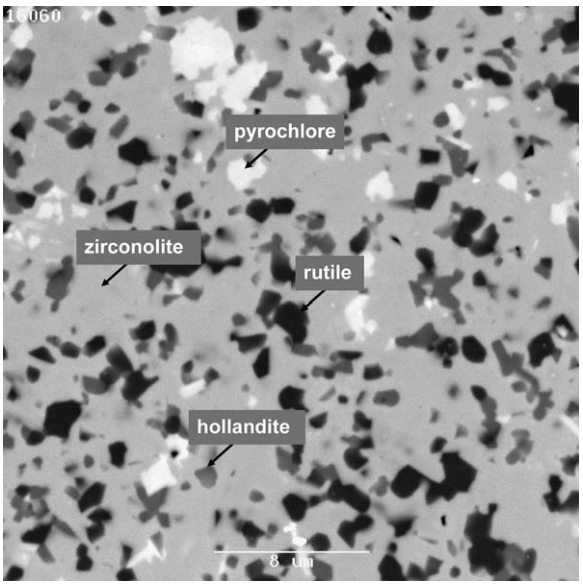

Fig. 1. SEM backscattered electron image of the synroc matrix (remote from the edges of the sample) showing four main phases.

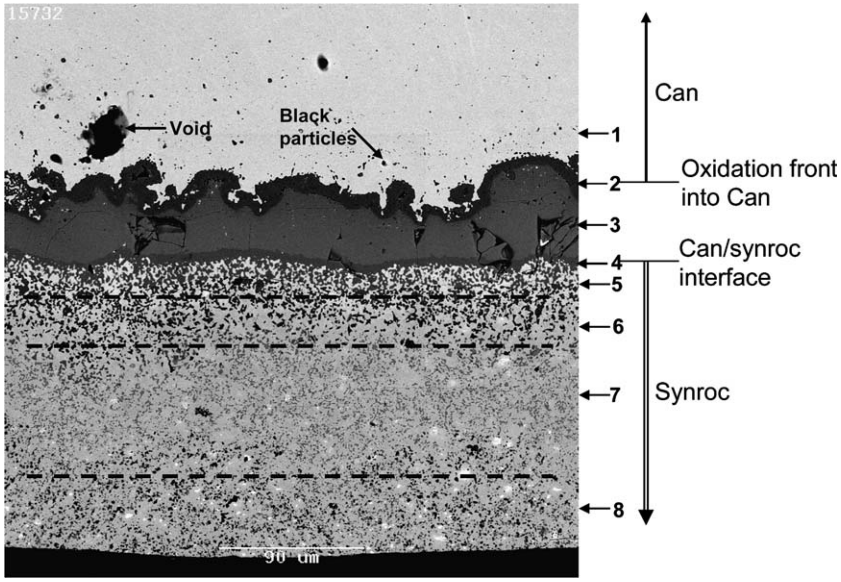

Fig. 2. SEM backscattered electron image of the interface region showing the eight distinct layers and black particles (Cr-oxide) in layer 1.

interface. The Ni concentration remained nearly constant. The black particles located in the metal (see Fig. 2) are Cr oxide (see Fig. 3).

Layer 2 is simply Cr-rich oxide (see Figs. 2 and 3, >95% Cr_2O_3 from EDS analysis) derived from the diffusion of Cr out of layer 1 and subsequent oxidation of the can material adjacent to the synroc. The composition is very uniform throughout the layer. The thickness of the layer varies from 10 to 20 μm. This is the oxidation front with the stainless steel can.

Layer 3 contains Fe- and Cr-rich oxides also derived from oxidation of the can material adjacent to the synroc and the compositions vary significantly with the distance from layer 2 (see Figs. 3 and 4) towards the synroc, from similar amounts of Fe and Cr oxides at the top of layer 3 adjacent to layer 2 (see Figs. 3 and 4) to mainly Fe-rich oxides approaching layer 4. Trace amounts of Al and Ti (<1%) were found in this layer, the result of Al and Ti diffusion from the synroc phases.

Layer 4, the original can/synroc interface, is a very thin (<10 μm) and uniform oxide layer rich in Fe with some Ni and Ti (see Table 3), formed as a result of direct reaction/interaction between the oxidised stainless steel and synroc.

Layers 5–8 are synroc-based layers. Layer 8 shows essentially the same microstructure as the bulk synroc matrix (see Figs. 1 and 2) but it is still contaminated, mainly with Fe (see below). Fig. 5 shows the detailed microstructures of layers 5–7. Layer 5 consists of two phases. The discontinuous dark grey phase is [Fe, Ti]-rich oxide, virtually the same in composition as layer 4. The light-colored phase is zirconolite, distributed throughout layers 5–6. Table 4 summarises the compositions of zirconolite in layers 5–8. The EDS analyses show that the Fe has diffused up to 300 μm into the synroc sample.

The dark phase in layer 6 is a [Fe, Ti]-rich complex oxide phase, probably Fe_2TiO_4. Table 5 lists its major elemental composition. It contains a much higher Ti content than the grey phase in layer 5.

Hollandite forms one of the major phases in layer 7 and layer 8. Table 6 summarises its composition in the different layers. The results clearly show that Fe is again the main element diffusing from the stainless steel and replacing Al in hollandite. This is to be expected as Fe–hollandites form [10]. The EDS analyses of pyrochlore in the two different layers show no significant composition variation, although their exact compositions were difficult to determine due to very small particle sizes.

It is evident that Fe is the main element diffusing from stainless steel into zirconolite and hollandite, which are the main phases in this synroc formulation, at the expense of Ca and Al.

3.2. The incorporation of Fe^{2+} into synroc phases

While no attempt was made to perform formal mass balance for the synroc/can interaction, it was clear that Fe plays the dominant role in the stainless

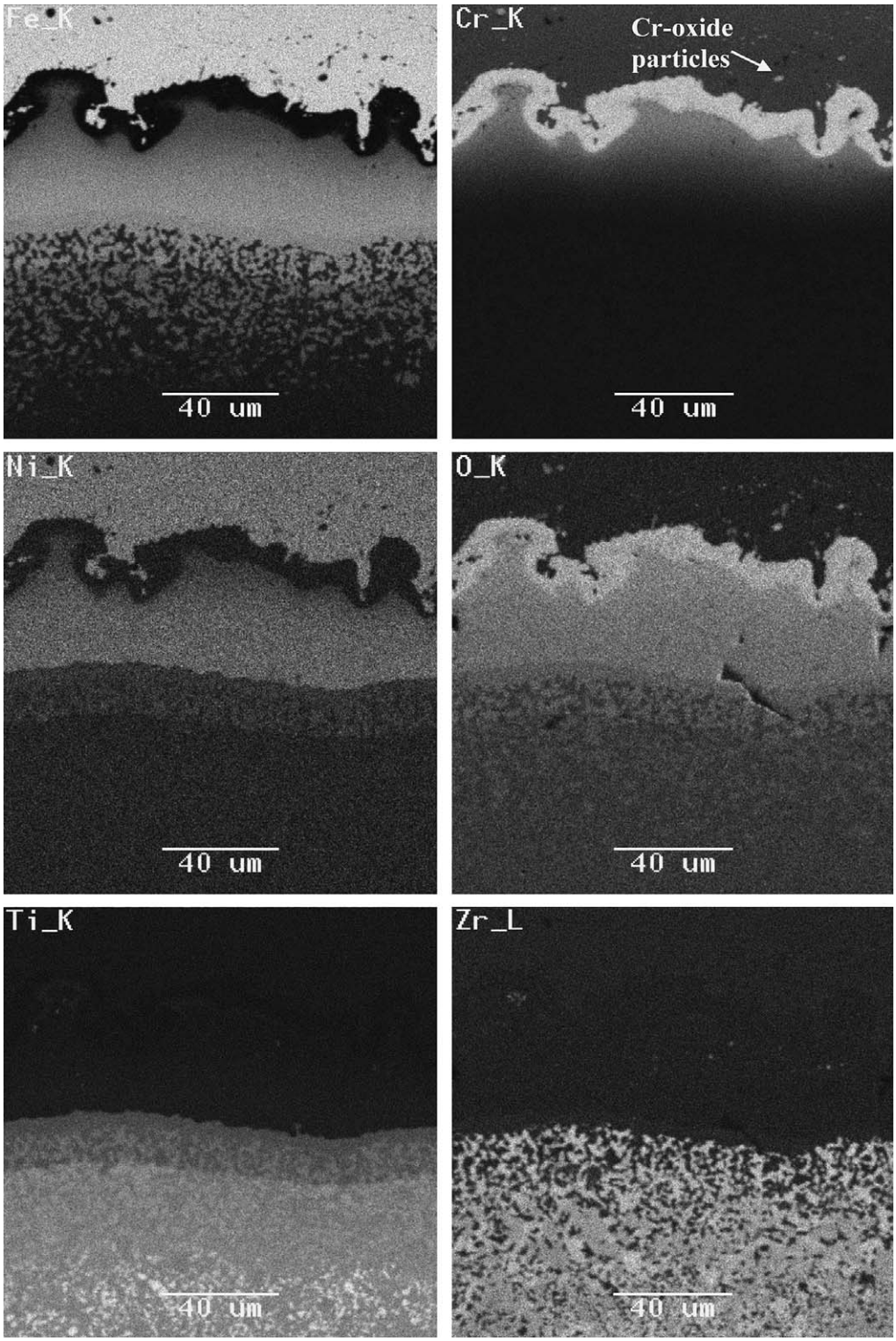

Fig. 3. Cross-sectional X-ray mapping of the interface region. The lighter the color, the more abundant is the element.

steel/synroc interactions during HIPing. Fe atoms have diffused about 300 μm into the synroc and changed the microstructure of the synroc phases in the top surface layers (layers 5–7). The overall

Table 2
The concentrations (wt%) of Fe, Cr and Ni in layer 1 as a function of distance from the interaction front towards the stainless steel matrix

	1 μm	10 μm	20 μm	30 μm	40 μm	50 μm	60 μm	70 μm	80 μm	90 μm	Matrix
Fe	78.0	78.7	78.4	78.5	77.0	75.3	74.5	71.9	72.7	72.6	70.4
Cr	11.5	10.3	11.3	12.6	13.5	15.5	16.2	17.0	17.6	17.8	18.5
Ni	9.3	9.9	9.6	8.1	8.2	8.0	7.7	8.3	7.8	7.5	8.3

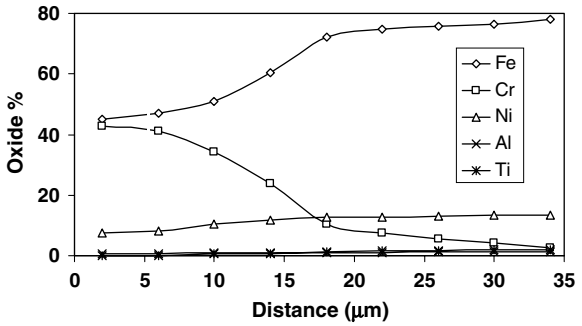

Fig. 4. Elemental profiles of oxides in layer 3 from the edge of layer 2 towards synroc side.

Table 3
Oxide composition (wt%) of layer 4, the grey phase

FeO	Cr_2O_3	NiO	Al_2O_3	TiO_2	HfO_2	ZrO_2	RE oxide
73.3	0.7	3.6	0.9	17.1	2.1	1.1	0.1

oxygen fugacity inside the HIP can is not known precisely but it will be driven by the stainless steel. This of course will favour the formation of Fe^{2+} rather than Fe^{3+} as an oxidation product. Fe^{2+} can enter both Ca and Ti sites of zirconolite. The maximum amounts of Fe^{2+} can enter the Ca site by the following reaction [11]:

$$0.9\ (CaZrTi_2O_7) + 0.14\ FeO + 0.28\ TiO_2 \rightarrow Ca_{0.90}Fe_{0.14}Zr_{0.90}Ti_{2.08}O_7 \quad (1)$$

The reaction consumes rutile as well. That partially explains the reason why there is very little rutile present in layers 5–6 where higher Fe^{2+} is present in zirconolite. Since the Fe contents of the layers

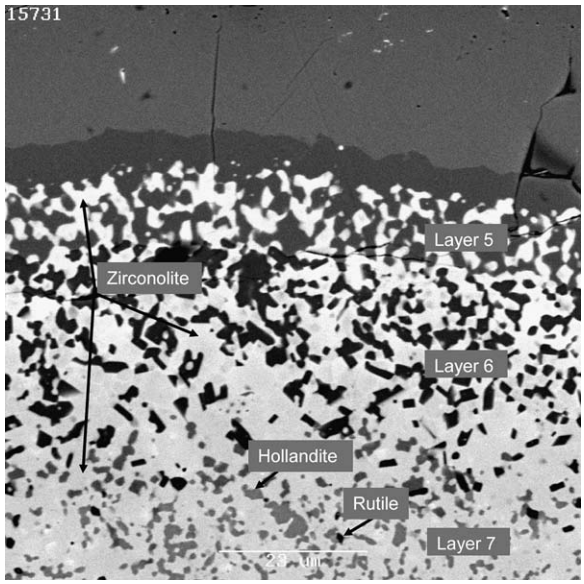

Fig. 5. SEM backscattered electron image showing detailed microstructures of the reaction layers 5–7.

5–7 greatly exceed the maximum Fe^{2+} stability in the Ca site of zirconolite, the majority of Fe^{2+} in zirconolite has entered the Ti site.

Both Fe^{2+} and Ti^{4+} can enter the Al site of hollandite ($Ba_xAl_{2x+y}Ti_{8-2x-\ y}O_{16}$) [10]. If $y/2(Fe^{2+} + Ti^{4+})$ are added to increase Fe^{2+} (y), the overall Ti^{4+} ($8-2x-y$) will correspondingly decrease. Therefore, adding Fe^{2+} to hollandite will effectively liberate Ti^{4+}, which is consistent with the coexistence of hollandite and rutile observed in layers 7–8. Furthermore, adding Fe^{2+} tends to form zirconolite at the expense of pyrochlore [12]. All

Table 4
Oxide composition (wt%) of zirconolite in the different layers

	FeO	Cr_2O_3	NiO	Al_2O_3	TiO_2	CaO	HfO_2	ZrO_2	RE_2O_3
Layer 5	12.3	0.1	0.1	0.5	29.4	4.6	2.3	28.5	24.9
Layer 6	9.8	0	0.4	2.2	31.3	4.9	1.3	23.3	25.0
Layer 7	6.7	0.1	0	2.9	35.6	6.4	1.8	22.5	22.0
Layer 8	2.3	0.2	0.1	3.7	33.2	7.2	1.6	26.7	22.0
Matrix	0	0	0	3.8	33.9	7.5	1.3	27.6	23.7

Table 5
Oxide composition (wt%) of the dark phase in layer 6

FeO	NiO	Al_2O_3	TiO_2	HfO_2	ZrO_2
57.0	1.5	2.8	34.5	0.1	3.0

Table 6
Oxide composition (wt%) of hollandite in the different layers

	FeO	Cr_2O_3	NiO	Al_2O_3	TiO_2	BaO
Layer 7	13.9	0.1	0.8	6.0	57.4	18.4
Layer 8	5.6	0.1	0.1	9.1	59.7	23.8
Matrix	0	0	0	13.6	59.9	23.2

these titanate phases are very chemically durable [10–12].

4. Conclusions

The interactions of stainless steel and synroc during HIPing gave rise to the formation of a complex interface region. The Fe diffusion controlled interactions have changed the synroc phase distribution in the upper interaction layers with more zirconolite present at the interface. However, the interactions do not produce any obvious less durable phases. Therefore the interactions are unlikely to have any detrimental effect on the stability and chemical durability of synroc as a high-level waste form, although more work is needed to fully elucidate the phase chemistry in the interaction zone.

Acknowledgements

We would like to thank G. Smith for sample preparation and R.A. Day for helpful discussions.

References

[1] A.E. Ringwood, S.E. Kesson, N.G. Ware, W. Hibberson, A. Major, Nature 278 (1979) 219.
[2] A.E. Ringwood, S.E. Kesson, K.D. Reeve, D.M. Levins, E.J. Ramm, in: W. Lutze, R.C. Ewing (Eds.), Radioactive Waste Forms for the Future, North-Holland, Amsterdam, 1988, p. 233.
[3] E.R. Vance, MRS Bull. 19 (1994) 12.
[4] B.D. Begg, E.R. Vance, B.A. Hunter, J.V. Hanna, J. Mater. Res. 13 (1997) 3181.
[5] E.R. Vance, A. Jostsons, R.A. Day, C.J. Ball, B. Begg, P.J. Angel, in: W.M. Murphy, D.A. Knecht (Eds.), Mat. Res. Soc. Symp. Proc. 412 (1996) 41.
[6] A. Jostsons, E.R. Vance, B. Ebbinghaus, Immobilization of surplus plutonium in titanate ceramics, Paper presented at Global 99, Jackson Hole, Wyoming, USA, 1999, August 29–September 3.
[7] R.A. Day, J. Ferenczy, E. Drabarek, T. Advocat, C. Fillet, J. Lacombe, C. Ladirat, C. Veyer, R. Do Quang, J. Thomasson, Glass-ceramics in a cold-crucible melter: the optimum combination for greater waste processing efficiency, in: WM'03 Conference, February 23–27, 2003, Tucson, AZ, USA.
[8] B.D. Begg, R.A. Day, S. Moricca, M.W.A. Stewart, E.R. Vance, Low-risk waste forms to lock up high-level nuclear waste, in: WM'05 Conference, February 27–March 3, 2005, Tucson, AZ, USA.
[9] G.R. Lumpkin, K.L. Smith, M.G. Blackford, R. Giere, C.T. Williams, Micron 25 (6) (1994) 581.
[10] M.L. Carter, R.L. Withers, J. Solid State Chem. 178 (2005) 1903.
[11] E.R. Vance, J.V. Hanna, B.A. Hunter, B.D. Begg, D.S. Perera, H. Li, Z. Zhang, Ceram. Trans. 143 (2003) 313.
[12] M.W.A. Stewart, E.R. Vance, R.A. Day, S. Leung, A. Brownscombe, M.L. Carter, B.B. Ebbinghaus, Impurity incorporation in pyrochlore-rich ceramics, in: G.T. Chandler, X. Feng (Eds.), 101st American ceramic society annual meeting, Indianapolis, April 25–28, 1999. Environmental Issues and Waste Management Technologies in the Ceramic and Nuclear Industries V, Ceram. Trans. 107 (2000) 569.